



Article

Multi-Objective Optimization of Base-Isolated Tanks with Supplemental Linear Viscous Dampers

Alexandros Tsipianitis and Yiannis Tsompanakis *

School of Chemical and Environmental Engineering, Technical University of Crete, 73 100 Chania, Greece

* Correspondence: jt@science.tuc.gr; Tel.: +30-28210-37634

Abstract: Base isolation of liquid storage tanks has proven to be an efficient seismic protection measure, leading to a drastic reduction of a superstructure's distress. However, many such tanks are located near seismic tectonic faults, which generate strong pulse-like ground motions that can impose excessive displacement demands on the isolators. For this reason, viscous dampers are incorporated into the isolation system to avoid overconservative isolators design. To optimize the seismic performance of hybrid isolation systems consisting of single friction pendulum bearings and linear viscous dampers, two novel multi-objective optimization approaches are proposed in the current study. Furthermore, suitable constraint functions and design variables are selected, considering the most critical parameters of the hybrid isolation system. The multi-objective genetic algorithm optimizer is used for the solution of both problems. The results are presented in the typical form of Pareto and certain optimal design solutions are carefully chosen and compared in terms of isolators fragility curves and tank accelerations. The main aim is to optimize the critical design parameters by achieving a reasonable balance among contradicting objectives. The tank industry can substantially benefit from this study, as a more cost-efficient design of hybrid base-isolation can be attained for large-scale tanks.

Keywords: liquid storage tanks; seismic vulnerability; seismic isolation; linear viscous dampers; multi-objective optimization



Citation: Tsipianitis, A.; Tsompanakis, Y. Multi-Objective Optimization of Base-Isolated Tanks with Supplemental Linear Viscous Dampers. *Infrastructures* **2022**, *7*, 157. <https://doi.org/10.3390/infrastructures7110157>

Academic Editor: Denise-Penelope N. Kontoni

Received: 29 September 2022

Accepted: 16 November 2022

Published: 17 November 2022

Publisher's Note: MDPI stays neutral with regard to jurisdictional claims in published maps and institutional affiliations.



Copyright: © 2022 by the authors. Licensee MDPI, Basel, Switzerland. This article is an open access article distributed under the terms and conditions of the Creative Commons Attribution (CC BY) license (<https://creativecommons.org/licenses/by/4.0/>).

1. Introduction

Liquid storage tanks are vital industrial infrastructures, as they are used to store hazardous chemicals and liquids, such as water, oil, and liquefied natural gas (LNG). These structures are very important due to their capacity to safely deliver the liquid content to the public even after disastrous events, such as earthquakes and tsunamis. Nonetheless, leakages, explosions, and tank wall damages were observed in liquid storage tanks in previous earthquakes, e.g., Northridge (1994), Kobe (1995), and Chi-Chi (1999), causing devastating consequences. Consequently, an efficient seismic design should be ensured to maintain their structural integrity for medium to strong earthquakes, because severe environmental problems and significant socioeconomic losses may result even from a minor failure.

An efficient approach to reduce the probability of failure of liquid storage tanks is the adoption of base-isolation technology [1]. The main goal of this design approach is to install seismic isolators at the base that “decouple” the superstructure from the imposed ground motions. These devices have low horizontal and high vertical stiffness to accommodate the structural weight. Due to the characteristics of the isolators, the displacements are increased due to their horizontal flexibility, while the structural accelerations and stresses are significantly reduced [2]. However, when a structure is located in near-fault areas, the displacement demands of the isolators may be notably increased due to the large-pulse characteristics of near-fault ground motions [3]. This problem can be solved in two possible ways: (a) by designing isolators with large displacement capacity or (b) by installing

supplemental damping devices at the base-isolated superstructure [4,5]. Obviously, the first approach may lead to overconservative and expensive designs, while the latter can achieve an improved seismic performance of the superstructure, if the hybrid system is properly designed.

Several studies have been devoted to the optimization of the seismic response of base-isolated structures, as well as base-isolated structural systems equipped also with supplemental dampers. For example, multi-objective genetic algorithms (MOGAs) were applied to optimize seismically isolated high-rise buildings by Pourzeynali and Zarif [6]. In particular, non-dominated sorting genetic algorithm (NSGA-II) was used to optimize the parameters of elastomeric isolators and to minimize the displacements of the building and the base isolation system. Shook et al. [7] proposed a hybrid base-isolation system that combined single friction pendulum bearings (SFPB), linear elastomeric bearings, magnetorheological (MR) dampers, and shape memory alloys (SMA). In addition, a multi-objective genetic algorithm was used to generate a fuzzy logic controller for the optimal evaluation of MR damper resistance levels. It was presented that base drifts were reduced by 18%, while the superstructure response was kept at allowable levels.

Taflanidis [8] implemented a stochastic subset optimization (SSO) algorithm focusing on the probabilistic design of supplemental dampers of bridge systems equipped with isolation bearings at the abutments and the piers. A significant improvement with respect to seismic vulnerability was observed when supplemental viscous dampers were installed. In the work of Ozbulut et al. [9], the adaptive control of structures isolated by laminated rubber bearings in combination with variable friction dampers (VFDs) was investigated. A multi-objective genetic algorithm was implemented for the learning process of an adaptive fuzzy neural controller. It was concluded that the seismic response of hybrid-isolated buildings was improved due to the proposed adaptive controllers. The NSGA-II scheme was implemented by Fallah and Zamiri [10] to improve the seismic response of base-isolated buildings based on a multi-objective formulation. The results indicated that the optimum values of isolators properties contributed to the effective suppress of superstructure's response. Moreover, it was reported that the addition of viscous dampers can improve the response of the base-isolated system. A multi-objective optimization was applied by Rizzian et al. [11] for the simultaneous consideration of a superstructure's elements (i.e., beams, column, reinforcements) and elastomeric device parameters (rubber type, size, maximum displacement capacity). It was concluded that the total building cost was significantly reduced due to base isolation. Etedali et al. [12] examined the multi-objective optimization of pure-friction isolators combined with a restoring device. The objectives were related to the reduction of superstructure accelerations and base displacements. According to the findings of this investigation, the base displacements were significantly reduced, while the residual displacements were diminished.

Regarding liquid storage tanks, Gregoriou et al. [13] performed dynamic analyses of LNG tanks protected via energy dissipating base-isolation systems. The results illustrated that base shear and maximum stresses were significantly reduced, while there were no significant differences regarding liquid sloshing phenomena compared to the case of fixed-base conditions. The effectiveness of a combined isolation system applied in a liquid storage tank was investigated by Weng et al. [14]. Following a performance-based framework, SFPB and viscous dampers parameters were examined for various seismic intensities and a tank's liquid filling percentage levels. When the friction coefficient presented low values and a higher amount of viscous damping was used, the seismic response of the tank was notably improved. An experimental base-isolated storage tank with friction bearings and elastoplastic dampers was also examined by Paolacci et al. [15]. It was shown that the seismic response could be improved up to 70% due to the hybrid isolation system.

Luo et al. [16] analyzed the impact of liquid sloshing in such critical infrastructure utilizing a hybrid control approach. It was found that by applying a hybrid isolation scheme, the maximum sloshing amplitudes of the liquid content of the tank, as well as the overturning moment and the base shear were significantly decreased. Khansefid et al. [17]

studied the optimum design of a combined isolation system consisting of a rubber isolator and rotational friction damper to enhance the seismic protection of LNG tanks. It was shown that the seismic response of the LNG tank was significantly improved and the damage probability was decreased, while the combined isolation system also contributed to the effective control of relative displacements. Labaf et al. [18] studied the multi-objective optimization of liquid storage tanks isolated by a hybrid control system (HCS) consisting of a base isolation system with a tuned mass inerter damper (TMID). The aim of the optimization was to design the HCS by minimizing the impulsive and convective displacements, as well as the base shear force. It was proven that the optimally designed HCS presented significantly reduced base shear, convective, and impulsive displacements, achieving reductions greater than 80% compared to conventional design.

Certainly, additional research is required to avoid failures, since many tanks located close to near-fault sites presented severe damages in past earthquakes (e.g., Izmit, Turkey). To the best of authors' knowledge, there is no relevant research that has presented a multi-objective optimization methodology for base-isolated liquid storage tanks equipped with supplemental dampers. In a recent work, Tsiipianitis and Tsompanakis [19] examined the seismic response of cylindrical steel tanks isolated via SFPB isolators and supplemental linear viscous dampers, but without considering any optimization framework. In addition, single-optimization formulations were proposed by Tsiipianitis and Tsompanakis [20] and Tsiipianitis et al. [21], aiming to optimize the seismic performance of base-isolated tanks without supplemental dampers, using standard and improved variants of Cuckoo Search optimizer.

In the current study, a suite of twenty near-fault accelerograms is used to test the optimized hybrid isolation system under strong impulses. Two different geometries (i.e., a squat and a slender tank) are examined, while for the efficient and accurate simulation of the liquid-tank response, a surrogate numerical model developed by Bakalis et al. [22] for fixed-base and later extended to base-isolated tanks [23] has been used. The main novelty of this work is the two multi-objective optimization approaches, consisting of three and four objective functions and appropriate design variables and constraints. More specifically, the friction coefficient and the radius of curvature of isolators and the damping coefficient of supplement dampers are the selected design variables, while the isolated system's damping and period are considered as the main constraint functions. The multi-objective genetic algorithm is utilized in both formulations, while the optimization results are presented in the form of multi-dimensional Pareto fronts, from which certain optimal design solutions are carefully chosen and compared in terms of isolators fragility curves and tank accelerations. The main aim is to optimize the critical design parameters by achieving a reasonable balance among contradicting objectives. The tank industry can substantially benefit from the multi-objective optimization approaches presented in this study, as a more cost-efficient design of hybrid base-isolation systems can be achieved for large-scale tanks.

2. Materials and Methods

2.1. Base Isolation and Supplemental Dampers

Base isolation systems with or without various types of dampers are frequently used in many engineering applications. Interested reader can seek for more information in Earthquake Protection Systems for isolation systems (<https://www.earthquakeprotection.com/>, accessed on 5 March 2016) and Taylor Devices for dampers (<https://www.taylordevices.com/>, accessed on 14 February 2018). In the current study, single friction pendulum bearings (SFPBs) are used for the base isolation of liquid storage tanks. SFPBs, which are also called single curved surface sliders (SCSSs), are efficient isolation devices that can significantly reduce the seismic vulnerability of structures and critical infrastructure [24]. It is a device with axisymmetric characteristics that uses its spherical geometrical setting to provide seismic isolation [25]. In addition, these isolators present two interesting characteristics: (a) the fundamental period and damping of the isolated superstructure do not

depend on the mass of the structure and (b) the center of rigidity coincides with the center of mass [25]. Due to this feature, the torsional response of the isolated superstructure is limited [26].

On the other hand, dampers are applied in structural systems to increase their energy dissipation capability. For this purpose, various types of energy dissipation devices have been developed, e.g., orificed-type viscous dampers (which have also been used in the current investigation), friction dampers, gap dampers, pressurized viscous dampers, etc. An important characteristic of viscous dampers is that damping forces are out of phase with the displacement-based forces in the structure; thus, the seismic loads do not generate increased forces for a sufficient level of structural deformation [27].

Therefore, an effective way to improve the seismic response of conventional buildings (e.g., museums, hospitals) and various infrastructure (e.g., bridges, liquid storage tanks) is to combine seismic isolators with supplemental viscous dampers. In particular, when such structures are located in near-fault sites, the displacement demands of the isolation system can be extremely high due to the long-period pulses of the imposed excitations. Consequently, the use of supplemental viscous dampers aims to: (a) reduce isolators' displacements to acceptable levels, (b) minimize the accelerations transmitted to the superstructure and reduce its distress, and (c) lead to a more cost-efficient design of the isolation system [28].

Hybrid schemes of isolators equipped with supplemental viscous dampers are often used in engineering practice aiming to efficiently protect various types of structures, such as the Rion-Antirion bridge, Greece (see Figure 1). Several researchers have studied the installation of supplemental dampers in conjunction with the isolators (e.g., [29]). For instance, Lafontaine et al. [30] assessed the impact of supplemental damping by examining of a base-isolated building using a set of isolators and magnetorheological (MR) dampers. In addition, elastomeric isolators in conjunction with viscous dampers were installed at buildings of Tohoku University in Japan. Detailed comparisons were made considering the same buildings with fixed-base conditions and various hybrid systems (i.e., high damping rubber bearings, lead rubber bearings with oil dampers, etc.) [31]. With reference to liquid storage tanks, Güler and Alhan [32] examined base-isolated liquid storage tanks with/without supplemental dampers under near-fault excitations. In addition, Castellano et al. [33] presented an experimental study of an LNG tank equipped with a hybrid system which consisted of elastomeric bearings and hysteretic dampers.



Figure 1. Supplemental viscous dampers installed in conjunction with elastomeric bearings in Rion-Antirion bridge, Greece.

2.2. Base Isolated Liquid Storage Tanks

2.2.1. Case Study Models and Design

In general, the simulation of the hydrodynamic response of the tank-liquid system is a complex and computationally demanding task. According to relevant studies (e.g., [32,34,35]), simplified models can be efficiently used for the dynamic analysis of seismically isolated storage tanks. In this work, the surrogate model developed by Bakalis et al. [22] has been used for the simulation of three-dimensional (3D) hybrid-isolated liquid storage tanks. The main component of this model is the beam-column element that carries the impulsive mass supported by rigid beam-spokes, which in turn are supported by the isolators and viscous dampers. For the two tank geometries examined herein (see Figure 2), the first model refers to a squat tank with slenderness ratio (i.e., liquid height-to-base radius) equal to $H/R = 0.67$, while the second represents a slender tank with $H/R = 3$. More details regarding the properties and the implementation of the examined simplified storage tank models can be found in [24].

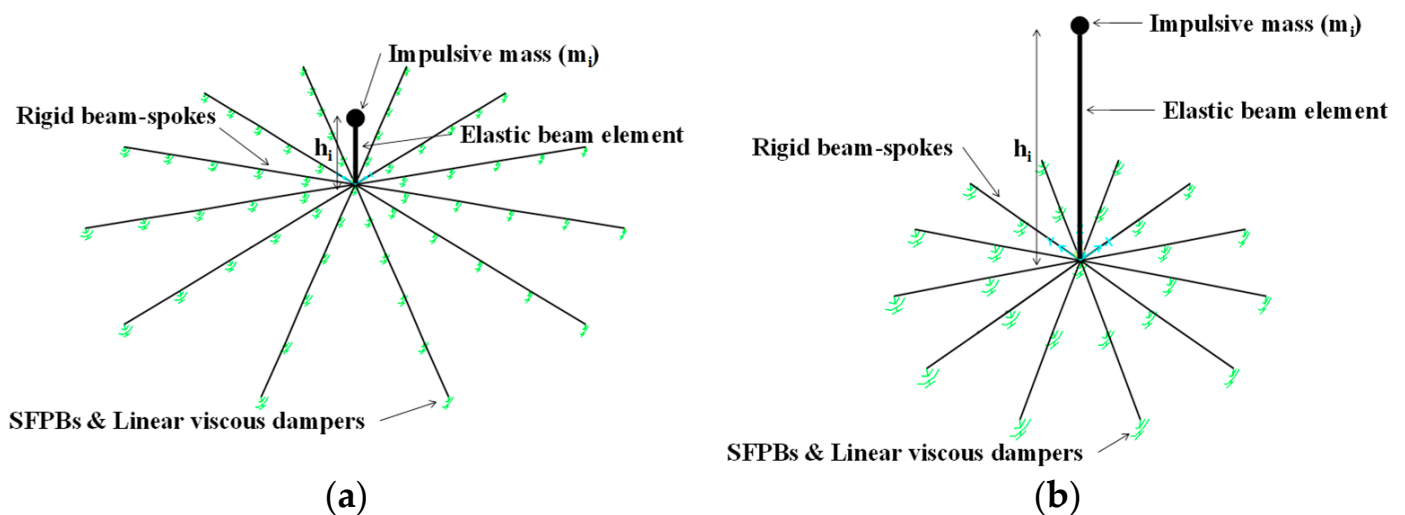


Figure 2. Simplified numerical models of: (a) the squat and (b) slender tank.

The validation of the numerical models is achieved by accurate matching of the impulsive fundamental period (T_i) according to the recommendations of Eurocode 8-Part 4 [36]. Many relevant studies have shown that the impulsive liquid mass dominates the hydrodynamic response of base-isolated liquid storage tanks, while the convective mass can be neglected [37,38]. In this simplified model, lumped masses at the base beam-spokes of the tanks represent the liquid weight. Additionally, the weight of tank wall is neglected, as it represents only 5% of the total tank mass [35].

2.2.2. Design of a Hybrid Isolation System

As described in the sequence, a base isolation system can be designed utilizing an iterative approach to determine isolation system parameters (e.g., effective stiffness, K_{eff} , effective damping, β_{eff} , etc.) for a certain friction coefficient, μ , and radius of curvature, R . Note that μ and R are either heuristically selected, or more efficiently derived utilizing one of the proposed optimization methodologies. The equivalent linear force (ELF) procedure is implemented for the design of the hybrid-isolated storage tanks, based on the recommendations of Eurocode 8 (for Soil A, $\gamma_i = 1.6$, $a_g = 0.36$ g). ELF is repeatedly applied, aiming to ensure that the SFPB capacity is equal to the target displacement. Otherwise, different design parameters are selected and the process is repeated.

It is noted that the impact of the dependence of friction coefficient on the sliding velocity can be ignored because the peak response of base-isolated storage tanks is not significantly affected [39]. Moreover, an experimental investigation by Constantinou et al. [40]

revealed that friction coefficient value is constant when sliding velocities present high values. This is also a valid assumption for the current study, due to the special frequency content of near-fault ground motions that exhibit significant velocity pulses. Lastly, the response of the vertical acceleration component is not considered herein due to the considerable resistance of steel tanks in the circumferential direction [41] and the trivial effect on the peak bearing displacement for long period (i.e., base-isolated) structures [42].

The minimum number of isolators for each tank is derived, based on the allowed maximum vertical load for each isolator, following the recommendations of Constantinou et al. [43]. Hence, as shown in Figure 2, 61 isolators are used in the squat storage tank, while 25 isolators are installed at the base of the slender tank. On the other hand, based on the applications of hybrid schemes presented in Section 2, viscous dampers are placed in parallel with the isolators, i.e., equal numbers of viscous dampers and isolators are applied. In addition, linear viscous dampers have been used, since previous studies [28,44] have proven that considering non-linear dampers does not alter the results. However, using exclusively linear viscous dampers is a limitation of this study; thus, non-linear dampers should also be examined in a future relevant investigation. Taylor device dampers with force capacity equal to 3000 kN have been selected. As explained in the sequence, the percentage of supplemental damping is derived within the optimization calculations. For each damper, the damping coefficient, c , is given by [45]:

$$n \cdot c = 2 \cdot \zeta \cdot \omega \cdot m = 2 \cdot \zeta \sqrt{\frac{n \cdot k_{isol}}{m}} \cdot m \Rightarrow c = \frac{2 \zeta \sqrt{n \cdot k_{isol} \cdot m}}{n} \tag{1}$$

where n is the number of SFPB isolators, ζ is the supplemental viscous damping [%], k_{isol} is the stiffness of each SFPB isolator [N/m], and m is the liquid mass [kg]. It should be noted that the vertical stiffness of the dampers is quite high (practically rigid) [46].

2.2.3. Dynamic Analysis and Earthquake Selection

The structural analysis program SAP2000 [47] is used for the modeling of a squat and slender tank supported on SFPB isolators and viscous dampers. In addition, the interface capability provided by the Application Programming Interface (API) is implemented with MATLAB programming software [48]. Regarding the imposed ground motions, twenty records from the near-fault database of FEMA/SAC Steel Project (https://nisee.berkeley.edu/elibrary/files/documents/data/strong_motion/sacsteel/motions/nearfault.html, accessed on 10 April 2017), listed in Table 1, are used to test the hybrid isolation system under large-pulse excitations. This is a widely applicable set of impulsive excitations, in which the closest distance from the fault ranges from 0 to 10 km for shallow crustal faults and from 6 to 18 km for blind thrust faults.

The Fast Non-linear Analysis (FNA) has been utilized in this investigation, as it is considered more computationally efficient than direct integration schemes. Moreover, it is suitable for structural systems in which the main non-linear response is related to the base isolation system, while the response of the superstructure remains in the elastic range [49,50]. One of the most critical aspects when applying FNA is the number of Ritz vector modes and the appropriate calculation of damping in order to avoid the detrimental phenomenon of “damping leakage” [24,50].

The incremental dynamic analysis (IDA) method is used for the scaling of the imposed near-fault ground motions [51]. In this manner, the dynamic behavior of the base-isolated storage tanks is examined by establishing a relation between the maximum response quantity, such as engineering demand parameter (EDP), and the seismic intensity level, which is represented by an intensity measure (IM). According to previous investigations (e.g., [52–54]), peak ground acceleration (PGA) has been selected, since it has been considered as a reliable IM for liquid storage tanks. Furthermore, the damping is set equal to 5% for the ultimate limit state of the tank [36] and 2% [55] for the impulsive liquid component.

Table 1. List of near-fault accelerograms.

No	SAC Ref	Record	Moment Magnitude	Distance (km)	PGA (g)	PGV (m/s)
#1	NF01	Tabas, 1978	7.4	1.2	0.90	1.13
#2	NF03	Loma Prieta, 1989, Los Gatos	7	3.5	0.72	1.36
#3	NF05	Loma Prieta, 1989, Lex. Dam	7	6.3	0.69	1.54
#4	NF07	C. Mendocino, 1992, Petrolia	7.1	8.5	0.64	1.41
#5	NF09	Erzincan, 1992	6.7	2	0.43	0.85
#6	NF11	Landers, 1992	7.3	1.1	0.71	0.95
#7	NF13	Northridge, 1994, Rinaldi	6.7	7.5	0.89	1.38
#8	NF15	Northridge, 1994, Olive View	6.7	6.4	0.73	1.01
#9	NF17	Kobe, 1995	6.9	3.4	1.09	1.68
#10	NF19	Kobe, 1995, Takatori	6.9	4.3	0.79	1.70
#11	NF21	Elysian Park 1	7.1	17.5	0.86	1.01
#12	NF23	Elysian Park 2	7.1	10.7	1.80	3.16
#13	NF25	Elysian Park 3	7.1	11.2	1.01	1.93
#14	NF27	Elysian Park 4	7.1	13.2	0.92	2.40
#15	NF29	Elysian Park 5	7.1	13.7	1.16	3.11
#16	NF31	Palos Verdes 1	7.1	1.5	0.97	2.71
#17	NF33	Palos Verdes 2	7.1	1.5	0.97	2.64
#18	NF35	Palos Verdes 3	7.1	1.5	0.87	2.15
#19	NF37	Palos Verdes 4	7.1	1.5	0.79	1.71
#20	NF39	Palos Verdes 5	7.1	1.5	0.92	2.26

In the present investigation, fragility curves in terms of SFPB maximum displacement (i.e., 0.305 m) are computed for the Maximum Credible Earthquake (MCE) with 2% probability of exceedance in 50 years, according to the methodology of fragility function fitting provided by Baker [56]. It should be stressed that the employed dampers do not reach their maximum capacity limit, i.e., 3000 kN. Therefore, isolator displacements constitute the critical capacity measure. Generally, the excessive horizontal deformation is considered as the main cause of isolators failures, in contrast to bearing uplift which is a very rare phenomenon [57]. Hence, fragility curves are derived in terms of exceedance of isolators' displacement capacity for all repetitively scaled ground motions.

2.2.4. Modeling of Link Elements

The “Friction isolator” non-linear link element available in SAP2000 has been used, which is a biaxial isolator that represents realistically the SFPB behavior. The two shear displacements and friction parameters are considered as coupled. Another significant characteristic of this link isolator element is the post-slip stiffness developed in the horizontal axes due to the radius of curvature of the sliding surface. Additionally, a gap behavior is exhibited in the translational direction, while linear-effective stiffness is included in the three moment deformations. Moreover, the proportionality of the compressive axial force with both friction and pendulum forces is considered [47].

On the other hand, the “Exponential Maxwell damper” element is utilized to simulate the operation of viscous dampers with linear or non-linear properties. The damping properties are determined for each degree of freedom based on the Maxwell viscoelasticity model [58], in which the following force-deformation relationship is used [47]:

$$f = k \cdot d_k = c \cdot d_c^{cexp} \tag{2}$$

where k is the spring constant (for the specific damper type: $k = 7.11 \times 10^{10}$ N/m), c represents the damping coefficient, d_k denotes the spring deformation, and d_c is the rate of damper deformation, while $cexp$ is the damping exponent that ranges between 0.2 and 2.0. In this work, $cexp = 1.0$, according to the recommendations of Hatzigeorgiou and Pnevmatikos [59] for linear viscous dampers.

2.3. Multi-Objective Optimization Formulations

In general, the majority of real-life problems include more than one design objective; thus, a multi-objective optimization approach can be more suitable than single-objective formulations. Moreover, in complex optimization problems, it may not be possible and/or efficient to combine the conflicting design objectives into a single objective function. Accordingly, a set of Pareto optimal solutions is derived when considering competitive objective functions. A constrained multi-objective optimization problem will have many feasible solutions, and the selection among them is achieved based on trade-offs among the objectives. Multi-objective optimization results (i.e., Pareto fronts) can be exploited by assigning proper weight factors to each optimization criterion and classify some Pareto solutions as more “attractive” than others. According to experts’ opinions from manufacturing companies, the proper (multi-objective) optimization formulation and selection among Pareto results can be extremely beneficial in order to achieve cost-efficient design of isolation systems [60].

Genetic algorithms (Gas), presented by Holland [61], are based on the evolution of biological systems according to Darwinian principles. The main operators used in GAs are: crossover, mutation, and selection of the fittest. This optimization scheme presents two significant advantages: (a) the effectiveness regarding complex problems and (b) the parallelism [62]. According to Pourzeynali and Zarif [6], GAs have been efficiently used in various engineering problems, including base-isolated structures (e.g., [11,63,64]). In this study, two multi-objective optimization formulations, the so-called MOGA1 and MOGA2, are proposed to determine the optimum parameters of a hybrid base-isolation system consisting of SFPB isolators and viscous dampers. More specifically, the Pareto optimal solution sets will be examined taking into account three (MOGA1) and four (MOGA2) objective functions. The results are derived in terms of radius of curvature, friction coefficient, and damping coefficient for each tank slenderness ratio (i.e., squat and slender). Appropriate bounds are set for the selected design variables of the SFPB isolators according to the recommendations of Zayas [65]: the friction coefficient ranges from 0.01 to 0.12, while the radius of the curvature ranges from 0.2032 m to 6.0452 m. In addition, the supplemental viscous damping ranges from 5% to 30%, as proposed in several studies (e.g., [45,66]).

Regarding the selected setup parameters of MOGA (which is applied utilizing Matlab optimization toolbox [48]) the population size is 200, while the “Creation function” that is used for the generation of new solutions and the “Mutation function” are both considered as “Constraint dependent”. The “Selection” is performed by “Tournament” scheme, while the “Crossover fraction” is chosen to be 0.8, i.e., 80% of the best designs are selected for “Crossover” and the remaining 20% for “Mutation” to produce the next generations [67]. Lastly, a limit of 2000 generations is set for the termination of the process.

As earlier mentioned, the optimization formulation of MOGA1 consists of three conflicting objective functions, while MOGA2 includes four objective functions, since a cost function is added in the formulation. More specifically, Equation (3), which represents the first objective function to be maximized, is derived from the integration of Equation (5) into (4) that describes the isolator effective stiffness, K_{eff} [N/m], and the damping coefficient, c_{VD} [Ns/m], respectively [25,45]:

$$c_{VD} = 2 \cdot \zeta \cdot \sqrt{\left(\frac{W}{R} + \mu \cdot \frac{W}{D}\right) \cdot m} \tag{3}$$

$$c_{VD} = 2 \cdot \zeta \cdot \sqrt{K_{eff} \cdot m} \tag{4}$$

$$K_{eff} = \frac{W}{R} + \mu \cdot \frac{W}{D} \tag{5}$$

where ζ is the supplemental viscous damping [%], K_{eff} is the stiffness of each SFPB [N/m], W denotes tank’s weight [N], μ is the friction coefficient, D denotes the maximum bearing displacement [m], R is the radius of curvature [m], and m is the tank-liquid mass [kg].

Subsequently, the second objective function (Equation (6)) refers to the minimization of accelerations, a [m/s^2], transmitted to the superstructure due to the presence of the base-isolation system, as proposed by Tsipianitis and Tsompanakis [20]:

$$a = \left(\frac{D}{R} + \mu \right) \cdot g \tag{6}$$

where g is the Earth’s gravity [m/s^2].

In addition, the third objective function (Equation (7)) aims at the minimization of maximum velocities, v_{max} [m/s], developed at the SFPB isolators [68]:

$$v_{max} = \frac{2 \cdot \pi \cdot D}{T_{SFPB}} \tag{7}$$

$$T_{SFPB} = 2 \cdot \pi \cdot \sqrt{\frac{1}{g \cdot \left(\frac{1}{R} + \frac{\mu}{D} \right)}} \tag{8}$$

which is obtained by combining Equations (7) and (8) as follows:

$$v_{max} = \frac{D}{\sqrt{g \cdot \left(\frac{1}{R} + \frac{\mu}{D} \right)}} \tag{9}$$

where T_{SFPB} denotes the SFPB isolator period [s].

Lastly, the fourth objective function—applied only in the case of MOGA2 formulation—is related to the cost of SFPB isolators, which is associated with the dimension and the capacity of the bearing [69]:

$$c = \exp(a(R) \cdot (D - 100)) \tag{10}$$

where $a(R) = 0.0002 \cdot R^2 - 0.0014 \cdot R + 0.0056$. The aim of this criterion is to examine the impact of the incorporation of the significant parameter of isolators cost in the multi-objective optimization formulation.

Constraint 1. The first constraint is related to isolators damping, β_{eff} . According to seismic provisions, damping should be within certain limits [70]:

$$\beta_{eff} = \frac{2 \cdot \mu}{\pi \cdot D_D + \mu} \text{ and } 0.2 \leq \beta_{eff} \leq 0.3 \tag{11}$$

where D_D is the design displacement of the isolator, which is set equal to 0.1 m, following Eurocode 8 guidelines [36]. By analyzing the lower and the upper bounds in Equation (11), the following two constraints are derived:

$$\beta_{eff} \leq 0.3 \Rightarrow \frac{2 \cdot \mu}{\pi \cdot \left(\frac{D_D}{R} + \mu \right)} \leq 0.3 \Rightarrow \mu - \frac{0.3 \cdot \pi \cdot D_D}{R \cdot (2 - 0.3 \cdot \pi)} \leq 0 \tag{12}$$

$$\beta_{eff} \geq 0.2 \Rightarrow \frac{2 \cdot \mu}{\pi \cdot \left(\frac{D_D}{R} + \mu \right)} \geq 0.2 \Rightarrow \frac{0.2 \cdot \pi \cdot D_D}{R \cdot (2 - 0.2 \cdot \pi)} - \mu \leq 0 \tag{13}$$

Constraint 2. An additional constraint is included in the optimization formulation, which is related to the period of the isolated superstructure:

$$T_{iso} = 2 \cdot \pi \cdot \sqrt{\frac{1}{g \cdot \left(\frac{1}{R} + \frac{\mu}{D} \right)}} \text{ and } 2 \text{ s} \leq T_{iso} \leq 3 \text{ s} \tag{14}$$

which, as previously, is transformed into two constraints:

$$T_{iso} \geq 2 s \Rightarrow \mu + D \cdot \left(\frac{1}{R} - \frac{\pi^2}{g} \right) \leq 0 \tag{15}$$

$$T_{iso} \leq 3 s \Rightarrow D \cdot \left(\frac{1}{0.228 \cdot g} - \frac{1}{R} \right) - \mu \leq 0 \tag{16}$$

Constraint 3. Lastly, the third constraint refers to the re-centering capability of SFPB isolators [71]:

$$\mu - \frac{D}{R} \leq 0 \tag{17}$$

The flowchart in Figure 3 highlights the main steps of multi-objective and dynamic analysis procedures. In particular, the central section of this flowchart presents the conventional approach, where isolator parameters have fixed values and specific values of supplemental damping are used (i.e., 5%, 10%, 20%, and 30%), without involving any optimization. On the other hand, the left and right parts correspond to MOGA1 and MOGA2 optimization formulations, respectively. As mentioned earlier, all dynamic analyses are implemented in SAP2000 software via API with MATLAB for the twenty near-fault accelerograms employing FNA and IDA methodologies, while the failure criterion is associated with the exceedance of maximum isolator displacement capacity. Lastly, the final part of the flowchart is related to the results, in terms of isolators fragility curves and the transmitted accelerations at the tank’s base. In addition, Table 2 lists the optimization objectives, constraints, and design variables for both approaches. It is noted that all isolators and dampers have the same parameter values in each design during the optimization process. Varying isolator and damper values could be examined in further investigations of the presented MOGA1 and MOGA2 approaches.

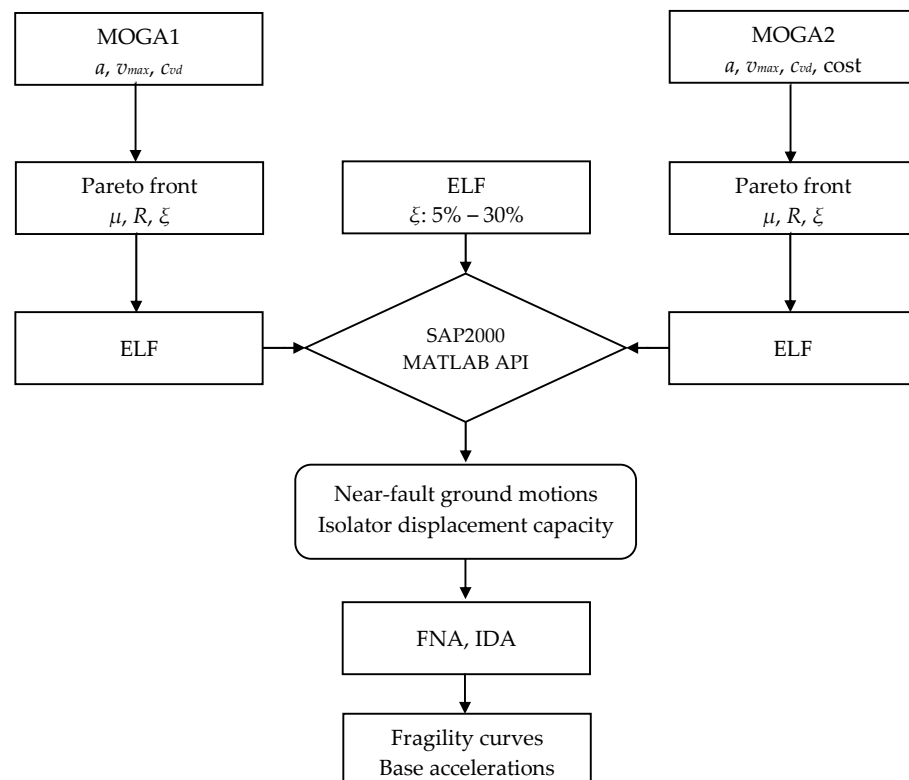


Figure 3. Flowchart of multi-objective optimization and dynamic analyses procedures.

Table 2. Summary of optimization objectives, constraints, and design variables.

Optimization Parameters	Expressions
Objective 1—Isolation damping coefficient	Maximize $c_{VD} = 2 \cdot \zeta \cdot \sqrt{\left(\frac{W}{R} + \mu \cdot \frac{W}{D}\right) \cdot m}$
Objective 2—Superstructure accelerations	Minimize $a = \left(\frac{D}{R} + \mu\right) \cdot g$
Objective 3—Maximum isolator velocity	Minimize $v_{max} = \frac{2 \cdot \pi \cdot D}{T_{SFPB}}$
Objective 4—Isolation cost	Minimize $c = \exp(a(R) \cdot (D - 100))$
Constraint 1—Isolation damping	$\beta_{eff} = \frac{2 \cdot \mu}{\pi \cdot D_D + \mu}$ and $0.2 \leq \beta_{eff} \leq 0.3$
Constraint 2—Isolated system period	$T_{iso} = 2 \cdot \pi \cdot \sqrt{\frac{1}{g \cdot \left(\frac{1}{R} + \frac{\mu}{D}\right)}}$ and $2 \text{ s} \leq T_{iso} \leq 3 \text{ s}$
Constraint 3—Isolator re-centering capability	$\mu - \frac{D}{R} \leq 0$
Design Variable 1—Friction coefficient	μ [0.01 0.12]
Design Variable 2—Radius of curvature	R [0.2032 m 6.0452 m]
Design Variable 3—Supplemental damping	ζ [5–30%]

3. Results and Discussion

3.1. MOGA1 Optimization Results

In this section, the results of the implementation of MOGA1 approach are presented. More specifically, Figure 4 depicts the 3D Pareto front results derived from the application of MOGA1 in each tank. In order to investigate the impact of the optimized hybrid isolation scheme on the seismic response of both tanks, four optimum design (OD) levels are selected according to the range of Pareto results, namely OD1, OD2, OD3, and OD4 solutions. The selection among Pareto results is based on the importance that is given to each one of the three objective functions included in MOGA1.

More specifically, OD1 and OD3 focus on optimizing the criterion related to acceleration and damping, respectively. On the other hand, OD2 and OD4 correspond to more balanced optimal solutions, in which the optimization of all objectives is considered to the maximum possible extend. This can be better understood in the 2D Pareto plots of Figure 4, which highlight more clearly the differences among the selected OD1, OD2, OD3, and OD4 solutions. Table 3 presents the values of the design variables and the three objective functions of MOGA1 for the four solutions for each tank. It can be easily observed that there are notable variations among the Pareto results of the two tanks, which affect the performance of the system and the superstructure, as shown in the following subsections.

Table 3. Optimization results for the selected solutions of the MOGA1 approach.

		μ	R [m]	ζ [%]	c_{VD} [kNs/m]	v_{max} [m/s]	a [m/s ²]
Squat tank	OD1	0.037	2.72	11	167.61	0.14	1.46
	OD2	0.041	1.75	16.5	280.12	0.12	2.11
	OD3	0.047	1.31	30	566.67	0.1	2.75
	OD4	0.044	2.28	25	408.62	0.13	1.75
Slender tank	OD1	0.038	2.78	9	110.62	0.14	1.45
	OD2	0.05	1.89	12	170.30	0.12	2.07
	OD3	0.046	1.22	28	431.87	0.1	2.9
	OD4	0.040	1.60	26	361.06	0.11	2.26

3.1.1. Isolators’ Fragility Curves

Figure 5 illustrates the fragility curves for each tank in terms of isolators’ displacement capacity of the selected four Pareto optimization solutions (i.e., OD1, OD2, OD3, OD4), compared with the hybrid isolation system results obtained in the authors’ previous

study [19], in which a constant value of supplemental damping was used (i.e., 5%, 10%, 20%, 30%) without implementing any optimization process, while SFPB had constant parameters ($R = 1.88$ m and $\mu = 0.08$) for all the examined cases. In contrast, different combinations of isolators parameters and damping coefficient values are derived in the current study, leading to a much more complicated response of the optimized hybrid system compared to the conventional configurations. As shown in Table 3, a significant variation can be observed in the resulting optimized design variable values (i.e., friction coefficient, radius of curvature and damping coefficient), which in turn affects the dynamic response of the whole system and the fragility estimates with respect to the displacement capacity exceedance of the friction bearings.

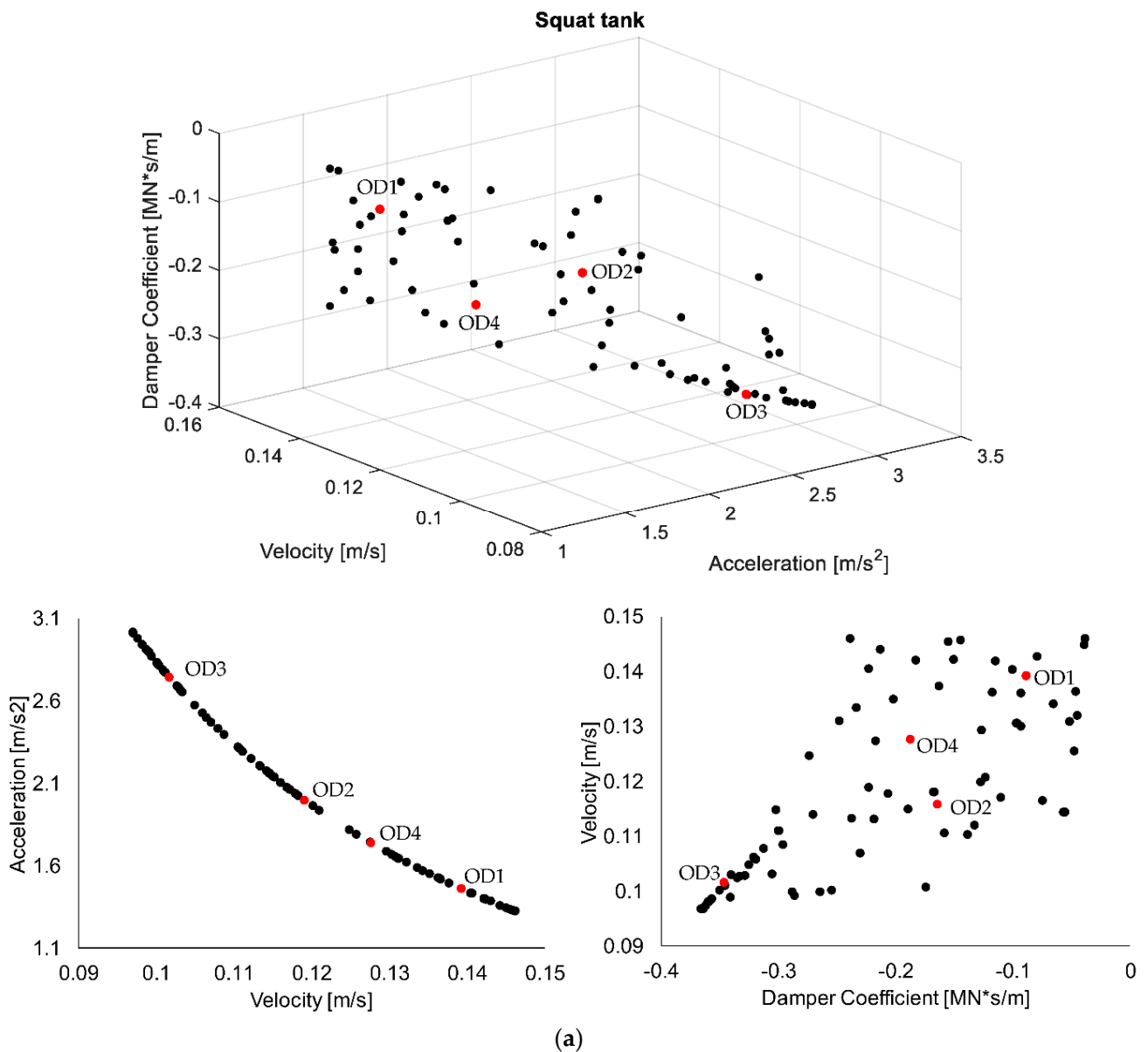


Figure 4. Cont.

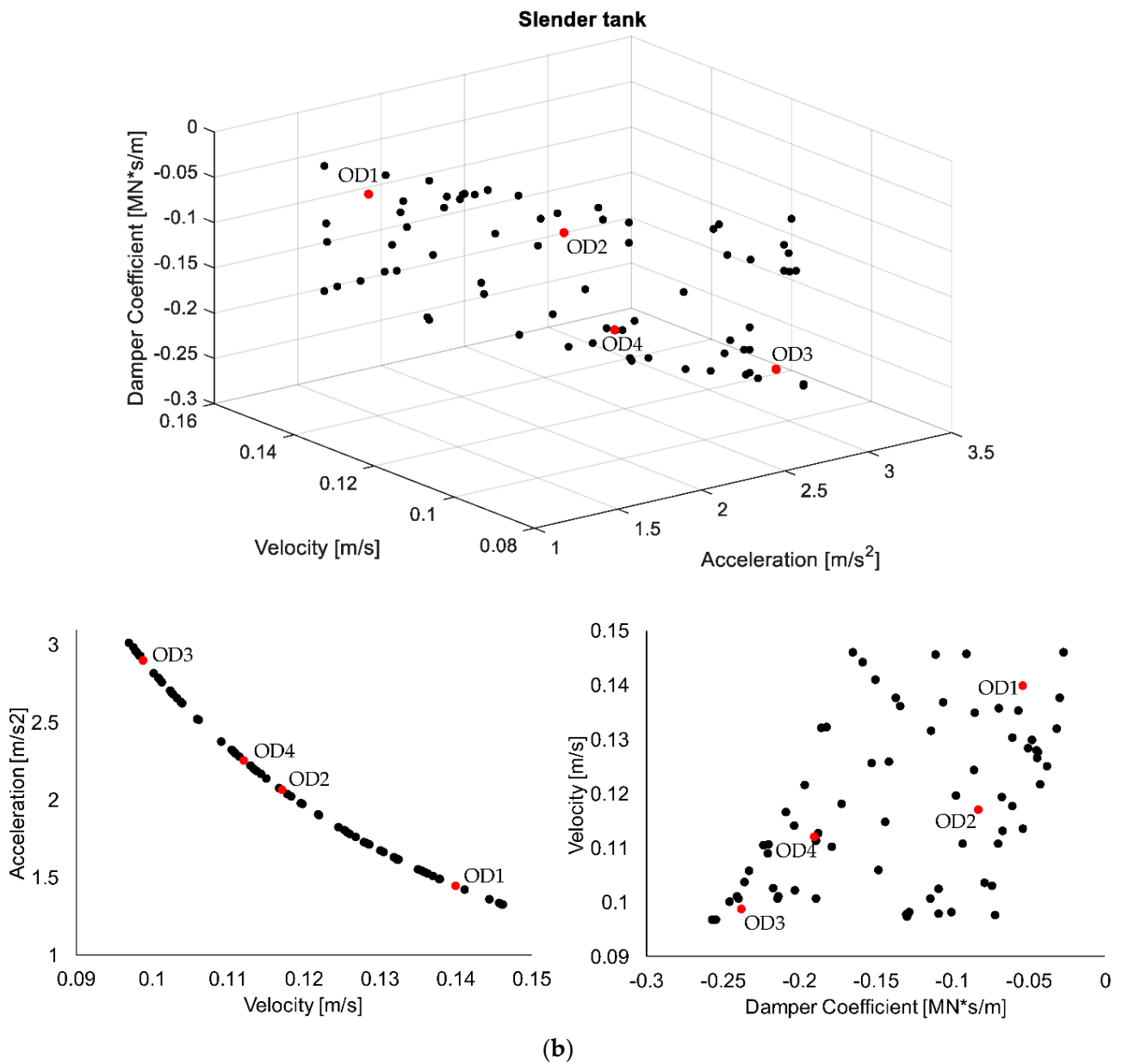


Figure 4. Three- and two-dimensional representations of Pareto front results regarding MOGA1 formulation for: (a) the squat and (b) slender tank.

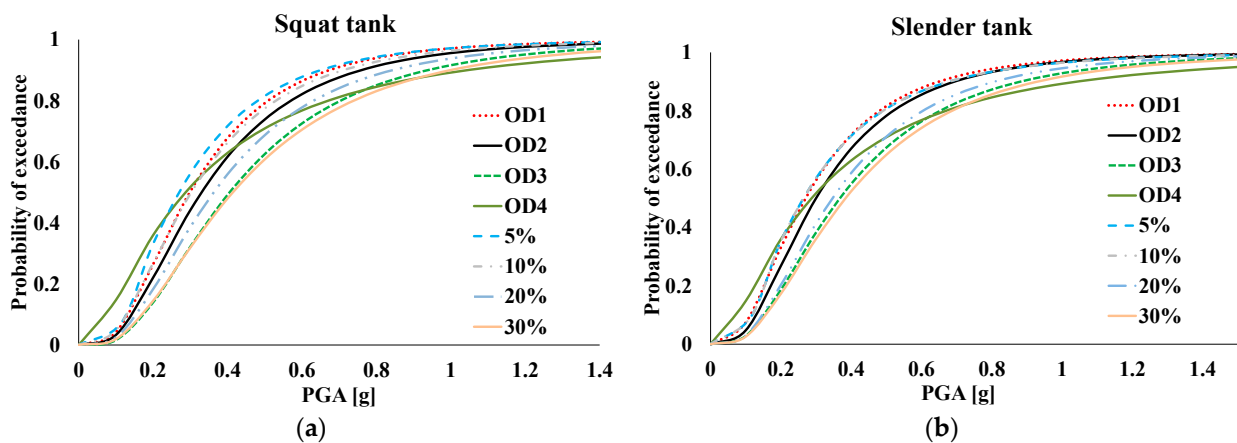


Figure 5. Fragility curves for MOGA1 designs for: (a) the squat and (b) slender tank.

In particular, the OD1 design presented the highest probabilities of exceedance for both tank slenderness ratios. The OD2 design produced slightly better results than OD1, especially for the squat tank. The best fragility results of the optimized hybrid configurations in the whole range of PGA values are derived for the OD3 design, in which the probabilities of exceedance—especially for PGA from 0.4 g to approximately 1 g—are notably lower than the other two approaches for both tanks. Lastly, OD4 presents quite different fragility results compared to the other three designs. More specifically, when PGA ranges from 0 to approximately 0.3 g, the probability of exceedance is higher. In contrast, for high PGA levels, the fragility results become progressively better than the other solutions.

In addition, the comparison of the fragility curves of the conventional hybrid isolated storage tanks [19] reveals that the optimized configuration OD3 presents almost identical fragility curves with the case of 30% supplemental damping for both squat and slender tanks. This is reasonable, taking into account that OD3 prioritizes damping maximization as close to the upper bound (i.e., 30%) as possible, as shown in the values listed in Table 3. Moreover, in the case of the slender tank (Figure 5b), the 20% curve is almost identical to 30% and OD3 curves, while similar results are observed for OD2, 5% and 10%, forming a group of two sets of results. With respect to the tank's geometry, it can be seen that the spacing among the fragility curves is less in the case of the slender tank, i.e., the fragility curves of the squat tank (Figure 5a) are more scattered. In future extensions of this study, different failure modes (e.g., tank wall buckling, excessive liquid sloshing, etc.) could be considered in the fragility analysis.

3.1.2. Superstructure Accelerations

A comparison is presented herein in terms of the accelerations transmitted to the superstructure, which are substantially reduced due to the presence of base-isolation in combination with supplemental dampers. This reduction enables the isolated tank to exhibit a linear response for the most frequently occurring range of PGA values; thus, tank wall damages and liquid content leakages can be avoided. Hence, as previously described, system failure is mainly associated with the exceedance of the allowable SFPB displacement capacity.

It is noted that the results for all the examined optimized and conventional hybrid designs shown in Figure 6 correspond to the maximum imposed values for every excitation of IDA scaling and dynamic analysis process, i.e., at the last step of the fragility analysis. It is clearly illustrated that the frequency content of each near-fault excitation plays a crucial role, which in conjunction with the selection of Pareto design has a considerable impact on the accelerations at the tanks' base (i.e., above the hybrid isolation system) for both geometries. More specifically, the lowest acceleration values are obtained in the case of OD1 design. The OD2 leads to slightly higher accelerations, while OD3 presents much higher values for certain accelerograms. Analogous to the fragility results, the OD4 solution exhibits a performance closer to OD3 design. In the case of OD4, high acceleration values are observed for both tank slenderness ratios for accelerogram #8 (i.e., NF15—Northridge record), while for OD3, the worst performance occurs for accelerograms #9 and #16.

With respect to the conventional supplemental viscous damping designs [19], the results of OD3 are almost identical with the corresponding ones for the conventional design with 30% of supplemental damping (especially for the squat tank (Figure 6a)), while OD1 results are identical to the lowest level of conventional supplemental damping (5%) for both tanks. Notable differences are observed in the ground motions that exhibit high acceleration values (records #9, #16, and #17) for both tank geometries.

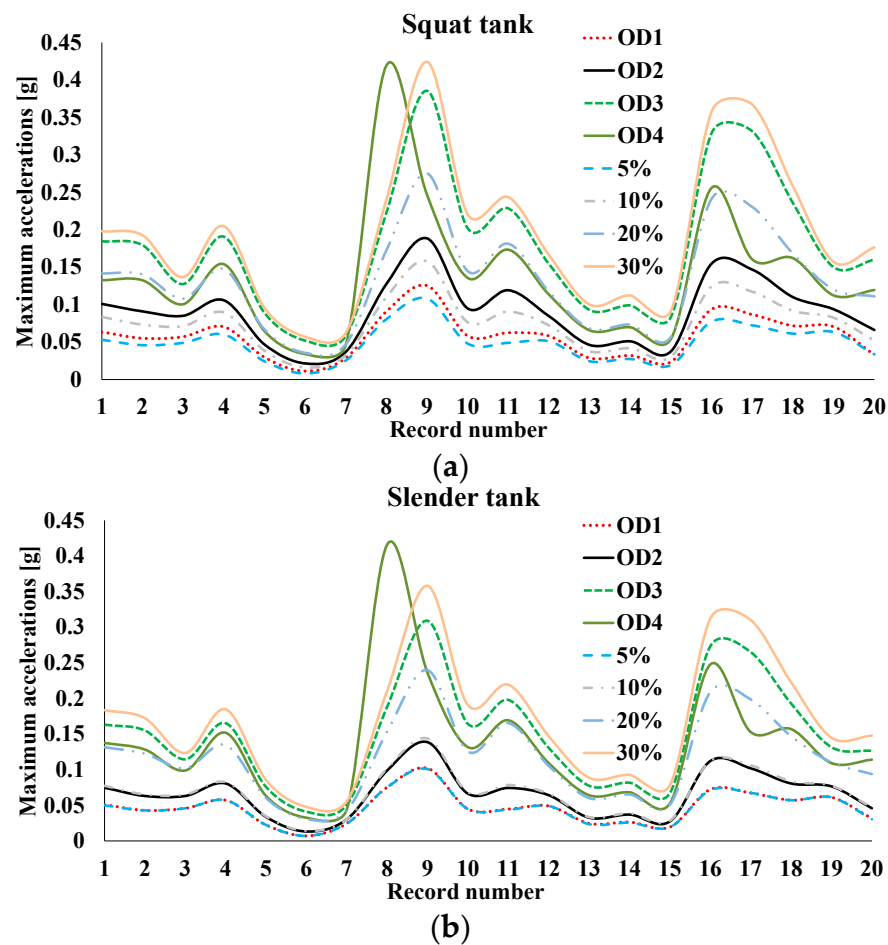


Figure 6. Accelerations at the tank base for: (a) the squat and (b) slender geometry.

3.2. MOGA2 Optimization Results

As previously described, the proposed MOGA2 optimization approach includes four objective functions, i.e., the three objective functions of MOGA1 and the additional cost function of SFPBs. This function was added in the formulation to enhance the cost-effectiveness of the approach, because several feasible designs can be extremely expensive. In order to present and understand the derived solutions of such complex multi-optimization implementation, the Pareto front results in Figure 7 are divided into three zones (low, medium, upper), in which several solutions are selected and compared (in terms of isolators fragility functions and tank base accelerations). It is noted that in MOGA2, the geometry is less influential than in MOGA1. More specifically, according to the scattering of the results, three optimized solutions have been selected for the low (LL, LM, and LR) and medium (ML, MM, and MR) zones, and two for the upper zone (HL and HR). As in the MOGA1 approach, the selection of these solutions has been based on the importance given to each objective function. For example, the LL design refers to minimized cost, damping, and acceleration, but a high value for velocity. On the other hand, the HR design corresponds to minimized velocity, but high values for acceleration, damping, and cost. Accordingly, the optimized values of the design variables are depicted in Table 4 for both tanks.

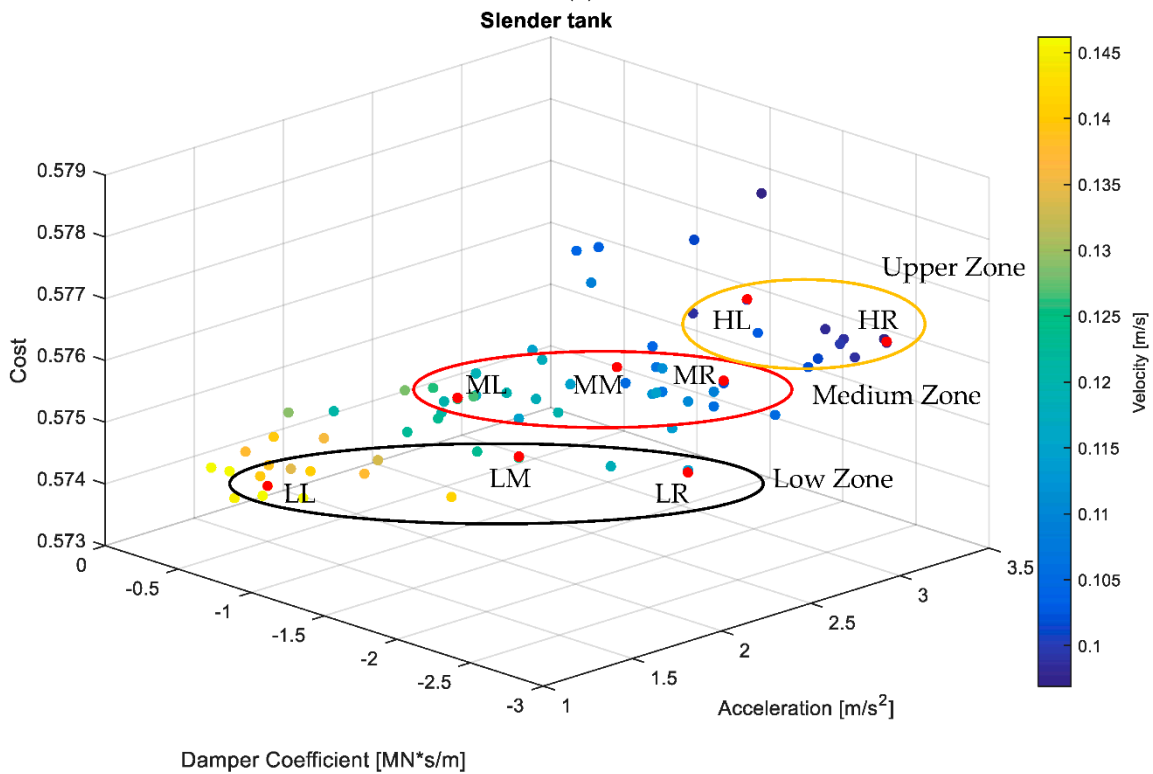
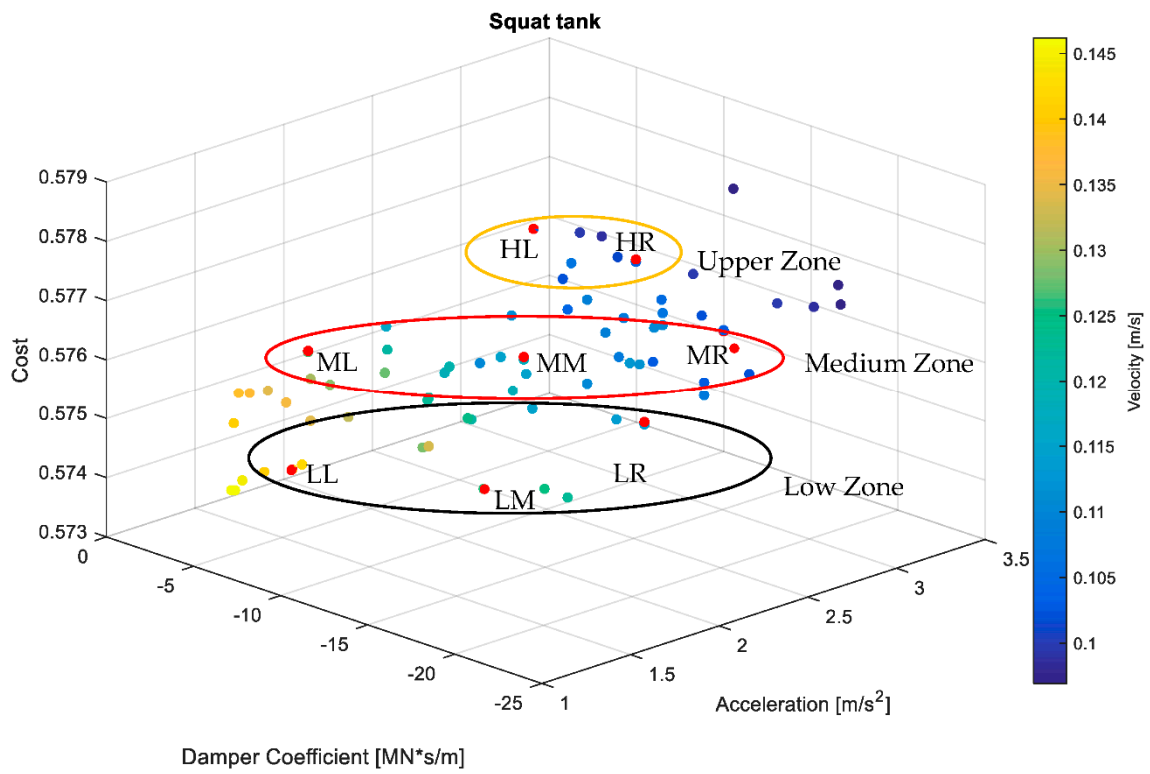


Figure 7. Pareto front results of MOGA2 formulation for: (a) the squat and (b) slender tank.

Table 4. Optimization results for the selected solutions of the MOGA2 approach.

	Optimized Level	μ	R [m]	ζ [%]	c_{VD} [kNs/m]
Squat tank	LL	0.027	2.52	12	171.42
	LM	0.028	1.98	23.9	362.91
	LR	0.042	1.66	29.6	512.33
	ML	0.045	2.27	7.2	118.69
	MM	0.051	1.90	22.3	394.83
	MR	0.056	1.39	26.3	512.90
	HL	0.065	1.48	20.2	219.98
	HR	0.064	1.45	11	404.61
Slender tank	LL	0.025	2.76	11	122.50
	LM	0.036	2.04	24.6	313.26
	LR	0.036	1.61	30	406.03
	ML	0.044	2.12	19	253.57
	MM	0.052	1.73	25	365.71
	MR	0.044	1.29	23	345.73
	HL	0.056	1.22	30	387.98
	HR	0.061	1.35	24	485.19

3.2.1. Isolators Fragility Curves

The fragility curves of the selected MOGA2 designs depicted in Figure 8 present differences depending on tank slenderness ratio and selected Pareto solution (e.g., LL, ML, etc.). More specifically, the results for the squat tank (Figure 8a) present more scattered curves, while the best fragility results are observed for LR and MR designs. On the other hand, the fragility curves of the slender tank (Figure 8b) are quite different from the same designs. For this geometry, the fragility curves are less scattered and can be grouped as follows: the first group with slightly better fragility results corresponds to HR and MR designs, the medium set refers to ML, LM, LR, and HL Pareto solutions, while LL presents the highest probabilities of exceedance.

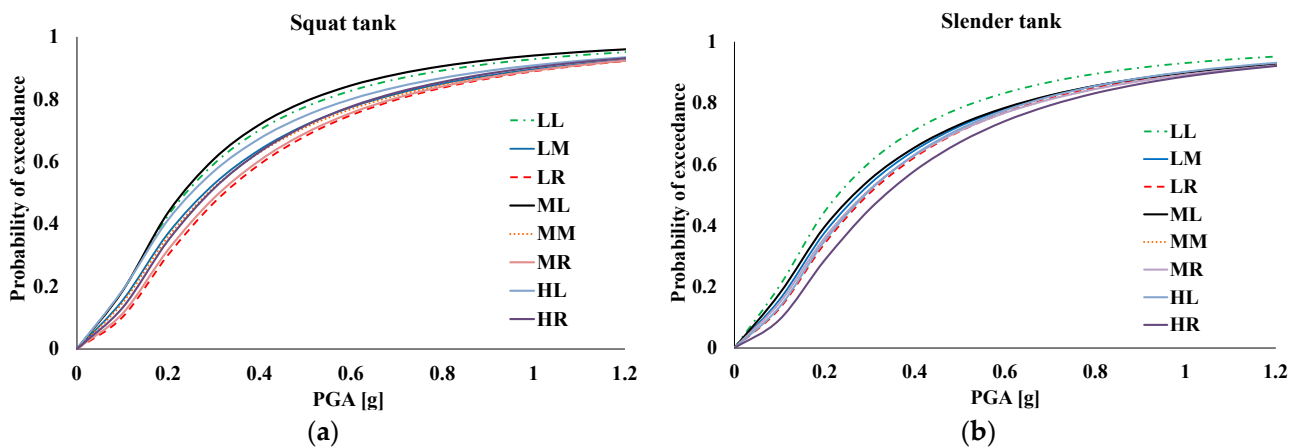


Figure 8. Fragility curves for MOGA2 designs for: (a) the squat and (b) slender tank.

In addition, Figure 9 presents a comparison among two Pareto solutions of the two multi-objective optimization approaches. A similar trend can be observed for both tank slenderness ratios, i.e., each multi-objective optimization solution outperforms the other depending on the PGA range. Regarding the squat tank (Figure 9a), OD3 design produces better fragility results for PGA less than 0.6 g, while LR presents slightly better results for PGA greater than 0.6 g. For the slender tank (Figure 9b), OD3 design leads to better fragility results for PGA less than 0.5 g, while LR exhibits a better performance for PGA greater than 0.5 g. Hence, MOGA2 is preferable for high seismic intensity levels, as it provides safer and more cost-efficient solutions.

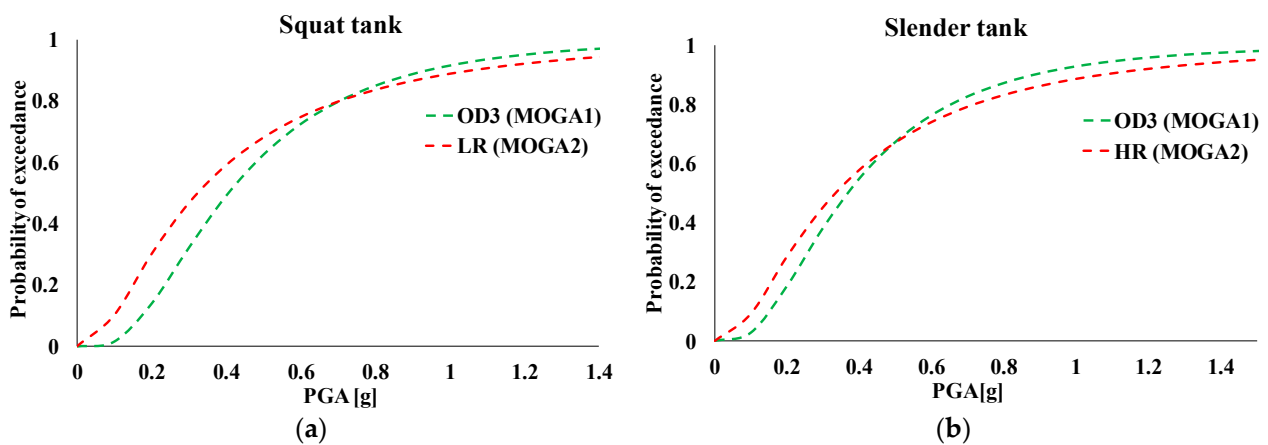


Figure 9. Comparison of MOGA1 and MOGA2 fragility curves for: (a) the squat and (b) slender tank.

3.2.2. Superstructure Accelerations

Figure 10 displays the transmitted accelerations to the tank’s base for the selected MOGA2 designs. Regarding the squat tank (Figure 10a), ML and LL designs present the lowest acceleration values, while LL, ML, and LM solutions present the lowest values for the slender tank (Figure 10b). Similar to MOGA1 results, the highest base acceleration values are observed for accelerograms #8 (i.e., NF15—Northridge record) and #16 (i.e., NF31—Palos Verdes 1 record) for both tank geometries.

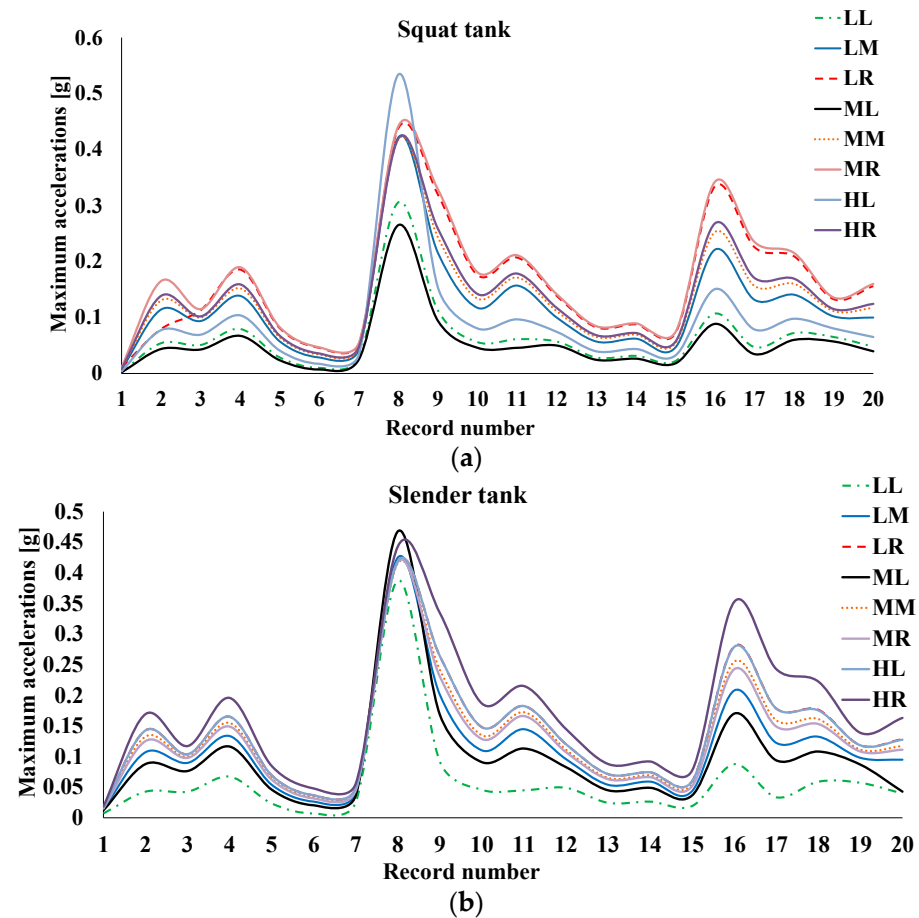


Figure 10. Accelerations at the tank base for: (a) the squat and (b) slender geometry.

4. Conclusions

In this paper, novel multi-objective optimization formulations have been presented, aiming to improve the dynamic performance of cylindrical steel tanks using optimized hybrid base-isolation schemes. More specifically, the examined squat and slender tanks have been isolated utilizing SFPB devices and supplemental linear viscous dampers, which have been optimized in an efficient multi-criteria manner. The MOGA1 optimization formulation consists of three objective functions which refer to the maximization of viscous damper stiffness, the minimization of superstructure accelerations, and isolators' maximum velocity, while in MOGA2, the cost function of SFPB isolators is also included in the optimization formulation. The friction coefficient, radius of curvature, and the percentage of supplemental damping have been considered as the design variables in both approaches. The constraint functions are related to the isolators effective damping and period, in conjunction with the re-centering capability of friction devices.

An efficient multi-objective genetic algorithm (MOGA) methodology based on GAS optimizer, i.e., NSGA-II, has been applied to perform the optimization calculations for both formulations. The obtained 3D Pareto front results have been carefully examined and categorized to select characteristic optimum designs for both MOGA1 and MOGA2 formulations. The dynamic performance, in terms of isolators fragility curves and accelerations transmitted to the superstructure, has been compared for both tank geometries, while conventionally designed hybrid systems (i.e., without optimization) have also been included in the comparisons. The following conclusions can be derived from the present investigation:

- MOGA constitutes an efficient optimization method for complex engineering real-life problems, such as liquid storage tanks equipped with a hybrid base-isolation system. The derived results for both formulations present significant variations for the optimized design variables values, depending on the importance given to each objective function, while the geometry of the tank also influences the results, especially in the case of MOGA1.
- With respect to MOGA1 optimization, the OD3 design presented the best fragility results, while the OD1 produced the lowest base accelerations. The OD2 design is chosen as the most efficient approach due to the compromise between fragility curves and the significantly reduced base accelerations.
- Regarding MOGA2 optimization, the HR design presented the best fragility results, while the LL provided the lowest base accelerations. The most efficient approach considering the best fragility curves and the lower base accelerations is the LM design.
- The comparison of optimization approaches has shown that MOGA2 is slightly superior to MOGA1 for higher seismic intensity levels (i.e., greater than 0.5 g) and vice versa.

Certainly, further investigation is required, including alternative objective and constraint functions in the optimization formulation to further improve the seismic response of hybrid-isolated tanks. Firstly, a comparison among multi-objective and single-objective optimization formulations could be performed. Additionally, the multi-objective optimization of liquid storage tanks isolated with other types of multi-stage friction pendulum bearings, such as Triple Friction Pendulum Bearings (TFPB) or Quintuple Friction Pendulum Bearings (QFPB), supplemental dampers (i.e., non-linear viscous dampers, friction dampers, viscous mass dampers, etc.), or adaptive negative stiffness systems [72] should also be examined.

Author Contributions: Conceptualization, A.T. and Y.T.; methodology, A.T. and Y.T.; software, A.T.; validation, A.T.; formal analysis, A.T.; investigation, A.T. and Y.T.; resources, A.T. and Y.T.; data curation, A.T.; writing—original draft preparation, A.T. and Y.T.; writing—review and editing, A.T. and Y.T.; visualization, A.T.; supervision, Y.T.; project administration, Y.T. All authors have read and agreed to the published version of the manuscript.

Funding: This research received no external funding.

Conflicts of Interest: The authors declare no conflict of interest. None funders had any role in the design of the study; in the collection, analyses, or interpretation of data; in the writing of the manuscript, or in the decision to publish the results.

References

1. Farajian, M.; Saeed, N.; Kang, W. Seismic Vulnerability Assessment of Base Isolated Liquid Storage Tanks under Near-Fault Ground Motions. *Structures* **2022**, *43*, 1901–1912. [[CrossRef](#)]
2. Shekari, M.R.; Khaji, N.; Ahmadi, M.T. On the Seismic Behavior of Cylindrical Base-Isolated Liquid Storage Tanks Excited by Long-Period Ground Motions. *Soil Dyn. Earthq. Eng.* **2010**, *30*, 968–980. [[CrossRef](#)]
3. Nigdeli, S.M.; Bekdaş, G.; Alhan, C. Optimization of Seismic Isolation Systems via Harmony Search. *Eng. Optim.* **2014**, *46*, 1553–1569. [[CrossRef](#)]
4. Çerçevik, A.E.; Avcı, Ö.; Hasançebi, O. Optimum Design of Seismic Isolation Systems Using Metaheuristic Search Methods. *Soil Dyn. Earthq. Eng.* **2020**, *131*, 106012. [[CrossRef](#)]
5. De Domenico, D.; Gandelli, E.; Quaglini, V. Adaptive Isolation System Combining Low-Friction Sliding Pendulum Bearings and SMA-Based Gap Dampers. *Eng. Struct.* **2020**, *212*, 110536. [[CrossRef](#)]
6. Pourzeynali, S.; Zarif, M. Multi-Objective Optimization of Seismically Isolated High-Rise Building Structures Using Genetic Algorithms. *J. Sound Vib.* **2008**, *311*, 1141–1160. [[CrossRef](#)]
7. Shook, D.A.; Roschke, P.N.; Ozbulut, O.E. Superelastic Semi-Active Damping of a Base-Isolated Structure. *Struct. Control Heal. Monit.* **2008**, *15*, 746–768. [[CrossRef](#)]
8. Taflanidis, A.A. Optimal Probabilistic Design of Seismic Dampers for the Protection of Isolated Bridges against Near-Fault Seismic Excitations. *Eng. Struct.* **2011**, *33*, 3496–3508. [[CrossRef](#)]
9. Ozbulut, O.E.; Bitaraf, M.; Hurlbauss, S. Adaptive Control of Base-Isolated Structures against near-Field Earthquakes Using Variable Friction Dampers. *Eng. Struct.* **2011**, *33*, 3143–3154. [[CrossRef](#)]
10. Fallah, N.; Zamiri, G. Multi-Objective Optimal Design of Sliding Base Isolation Using Genetic Algorithm. *Sci. Iran.* **2013**, *20*, 87–96. [[CrossRef](#)]
11. Rizzian, L.; Léger, N.; Marchi, M. Multiobjective Sizing Optimization of Seismic-Isolated Reinforced Concrete Structures. *Procedia Eng.* **2017**, *199*, 372–377. [[CrossRef](#)]
12. Etedali, S.; Hasankhoie, K.; Sohrabi, M.R. Optimal Design of Pure-Friction Isolators with and without Restoring Device: A Multi-Objective Cuckoo Search-Based Approach for Seismic-Excited Structures. *Structures* **2020**, *25*, 708–719. [[CrossRef](#)]
13. Gregoriou, V.P.; Tsinopoulos, S.V.; Karabalis, D.L. Dynamic Analysis of Liquefied Natural Gas Tanks Seismically Protected with Energy Dissipating Base Isolation Systems. In Proceedings of the ECCOMAS Thematic Conference—COMPDYN 2011: 3rd International Conference on Computational Methods in Structural Dynamics and Earthquake Engineering: An IACM Special Interest Conference, Programme, Corfu, Greece, 25–28 May 2011.
14. Weng, D.; Zhang, R.; Ge, Q.; Liu, S. Effect Investigation of Combination Isolation System for Liquid Storage Tank in Different Seismic Levels. In Proceedings of the 15th World Conference on Earthquake Engineering (15WCEE), Lisbon, Portugal, 24–28 September 2012.
15. Paolacci, F.; Giannini, R.; De Angelis, M. Seismic Response Mitigation of Chemical Plant Components by Passive Control Techniques. *J. Loss Prev. Process Ind.* **2013**, *26*, 924–935. [[CrossRef](#)]
16. Luo, H.; Zhang, R.; Weng, D. Mitigation of Liquid Sloshing in Storage Tanks by Using a Hybrid Control Method. *Soil Dyn. Earthq. Eng.* **2016**, *90*, 183–195. [[CrossRef](#)]
17. Khansefid, A.; Maghsoudi-Barmi, A.; Khaloo, A. Seismic Protection of LNG Tanks with Reliability Based Optimally Designed Combined Rubber Isolator and Friction Damper. *Earthq. Struct.* **2019**, *16*, 523–532. [[CrossRef](#)]
18. Labaf, D.Z.; De Angelis, M.; Basili, M. Multi-objective Optimal Design and Seismic Assessment of an Inerter-based Hybrid Control System for Storage Tanks. *Bull. Earthq. Eng.* **2022**, *43*, 1091–1099. [[CrossRef](#)]
19. Tsiapanitis, A.; Tsompanakis, Y. Improving the Seismic Performance of Base-Isolated Liquid Storage Tanks with Supplemental Linear Viscous Dampers. *Earthq. Eng. Eng. Vib.* **2022**, *21*, 269–282. [[CrossRef](#)]
20. Tsiapanitis, A.; Tsompanakis, Y. Optimizing the Seismic Response of Base-Isolated Liquid Storage Tanks Using Swarm Intelligence Algorithms. *Comput. Struct.* **2021**, *243*, 106407. [[CrossRef](#)]
21. Tsiapanitis, A.; Spachis, A.; Tsompanakis, Y. Combined Optimization of Friction-Based Isolators in Liquid Storage Tanks. *Appl. Sci.* **2022**, *12*, 9879. [[CrossRef](#)]
22. Bakalis, K.; Fragiadakis, M.; Vamvatsikos, D. Surrogate Modeling for the Seismic Performance Assessment of Liquid Storage Tanks. *J. Struct. Eng.* **2017**, *143*, 04016199. [[CrossRef](#)]
23. Bakalis, K.; Vamvatsikos, D.; Grant, D.N.; Mistry, A. Downtime Assessment of Base-Isolated Liquid Storage Tanks. In Proceedings of the 2019 SECED Conference: Earthquake Risk and Engineering towards a Resilient World, London, UK, 9–10 September 2019; pp. 1–10.
24. Tsiapanitis, A.; Tsompanakis, Y. Impact of Damping Modeling on the Seismic Response of Base-Isolated Liquid Storage Tanks. *Soil Dyn. Earthq. Eng.* **2019**, *121*, 281–292. [[CrossRef](#)]
25. Zayas, V.; Low, S.; Mahin, S. *The FPS Earthquake Resisting System*; EERC Report No. UCB/EERC-87/01; University of California: Berkeley, CA, USA, 1987.

26. Furinghetti, M.; Pavese, A. Definition of a Simplified Design Procedure of Seismic Isolation Systems for Bridges. *Struct. Eng. Int.* **2020**, *30*, 381–386. [[CrossRef](#)]
27. Lago, A.; Trabucco, D.; Wood, A. An Introduction to Dynamic Modification Devices. In *Damping Technologies for Tall Buildings*; Elsevier B.V.: Amsterdam, The Netherlands, 2019; pp. 107–234. [[CrossRef](#)]
28. Lu, L.Y.; Lin, C.C.; Lin, G.L. Experimental Evaluation of Supplemental Viscous Damping for a Sliding Isolation System under Pulse-like Base Excitations. *J. Sound Vib.* **2013**, *332*, 1982–1999. [[CrossRef](#)]
29. Taylor, D.P. History, Design, and Applications of Fluid Dampers in Structural Engineering. In Proceedings of the Passive Structural Control Symposium, Tokyo, Japan, 13–14 December 2002; pp. 17–34.
30. Lafontaine, M.; Moroni, O.; Sarrazin, M.; Roschke, P. Optimal Control of Accelerations in a Base-Isolated Building Using Magneto-Rheological Dampers and Genetic Algorithms. *J. Earthq. Eng.* **2009**, *13*, 1153–1171. [[CrossRef](#)]
31. Kaneko, M.; Tamura, K.; Maebayashi, K.; Sarnta, M. Earthquake response characteristics of base-isolated buildings. In Proceedings of the 4th US National Conference of Earthquake Engineering, Palm Springs, CA, USA, 20–24 May 1990; pp. 569–578.
32. Güler, E.; Alhan, C. Performance Limits of Base-isolated Liquid Storage Tanks with/without Supplemental Dampers Under Near-fault Earthquakes. *Structures* **2021**, *33*, 355–367. [[CrossRef](#)]
33. Castellano, M.G.; Infanti, S.; Dumoulin, C.; Ducoup, L.; Martelli, A.; Dusi, A. Shaking Table Tests on a Liquefied Natural Gas Storage Tank Mock-up Seismically Protected with Elastomeric Isolators and Steel Hysteretic Torsional Dampers. In Proceedings of the 12th World Conference on Earthquake Engineering, Auckland, New Zealand, 30 January–4 February 2000; pp. 1–8.
34. De Angelis, M.; Giannini, R.; Paolacci, F. Experimental Investigation on the Seismic Response of a Steel Liquid Storage Tank Equipped with Floating Roof by Shaking Table Tests. *Earthq. Eng. Struct. Dyn.* **2010**, *39*, 377–396. [[CrossRef](#)]
35. Uckan, E.; Umut, Ö.; Sisman, F.N.; Karimzadeh, S.; Askan, A. Seismic Response of Base Isolated Liquid Storage Tanks to Real and Simulated near Fault Pulse Type Ground Motions. *Soil Dyn. Earthq. Eng.* **2018**, *112*, 58–68. [[CrossRef](#)]
36. CEN. *Eurocode 8—Design of Structures for Earthquake Resistance—Part 4: Silos, Tanks and Pipelines EN 1998-4*; European Committee for Standardization: Brussels, Belgium, 2006.
37. Paolacci, F. On the Effectiveness of Two Isolation Systems for the Seismic Protection of Elevated Tanks. *J. Press. Vessel Technol. Trans. ASME* **2015**, *137*, 031801. [[CrossRef](#)]
38. Rawat, A.; Matsagar, V.A.; Nagpal, A.K. Numerical Study of Base-Isolated Cylindrical Liquid Storage Tanks Using Coupled Acoustic-Structural Approach. *Soil Dyn. Earthq. Eng.* **2019**, *119*, 196–219. [[CrossRef](#)]
39. Pranesh, M.; Sinha, R. VFPI: An Isolation Device for Aseismic Design. *Earthq. Eng. Struct. Dyn.* **2000**, *29*, 603–627. [[CrossRef](#)]
40. Constantinou, M.; Mokha, A.; Reinhorn, A. Teflon Bearings in Base Isolation II: Modeling. *J. Struct. Eng.* **1990**, *116*, 455–474. [[CrossRef](#)]
41. Haroun, M.A.; Tayel, M.A. Response of Tanks to Vertical Seismic Excitations. *Earthq. Eng. Struct. Dyn.* **1985**, *13*, 583–595. [[CrossRef](#)]
42. Loghman, V.; Khoshnoudian, F.; Banazadeh, M. Effect of Vertical Component of Earthquake on Seismic Responses of Triple Concave Friction Pendulum Base-Isolated Structures. *JVC/J. Vib. Control.* **2015**, *21*, 2099–2113. [[CrossRef](#)]
43. Constantinou, M.C.; Kalpakidis, I.; Filiatrault, A.; Lay, R.A.E. *LRFD-Based Analysis and Design Procedures for Bridge Bearings and Seismic Isolators*; University at Buffalo: New York, NY, USA, 2011.
44. Wolff, E.D.; Ipek, C.; Constantinou, M.C.; Tapan, M. Effect of Viscous Damping Devices on the Response of Seismically Isolated Structures. *Earthq. Eng. Struct. Dyn.* **2015**, *44*, 185–198. [[CrossRef](#)]
45. Provdakis, C.P. Effect of Supplemental Damping on LRB and FPS Seismic Isolators under Near-Fault Ground Motions. *Soil Dyn. Earthq. Eng.* **2009**, *29*, 80–90. [[CrossRef](#)]
46. Taylor, A.W. Response Control Systems in the United States and Lessons Learned from the Tohoku Earthquake. In Proceedings of the International Symposium on Engineering Lessons Learned from the 2011 Great East Japan Earthquake, Tokyo, Japan, 1–4 March 2012; pp. 1087–1098.
47. CSI Computers and Structures Inc. *SAP2000*, Version 20. Integrated Software for Structural Analysis and Design, Analysis Reference Manual. Computers and Structures Inc.: Berkeley, CA, USA, 2017.
48. Mathworks, Inc. *MATLAB & Optimization Toolbox R2015a*; The Mathworks, Inc.: Natick, MA, USA.
49. Sorace, S.; Terenzi, G. Analysis and Demonstrative Application of a Base Isolation/Supplemental Damping Technology. *Earthq. Spectra* **2008**, *24*, 775–793. [[CrossRef](#)]
50. Sarlis, A.A.; Constantinou, M.C. Modeling triple friction pendulum isolators in program SAP2000. In *Document Distributed to the Engineering Community Together with Example*; Department of Civil, Structural and Environmental Engineering, University at Buffalo, State University of New York: Buffalo, NY, USA, 2010.
51. Vamvatsikos, D.; Allin Cornell, C. Incremental Dynamic Analysis. *Earthq. Eng. Struct. Dyn.* **2002**, *31*, 491–514. [[CrossRef](#)]
52. Saha, S.K.; Matsagar, V.; Chakraborty, S. Uncertainty Quantification and Seismic Fragility of Base-Isolated Liquid Storage Tanks Using Response Surface Models. *Probabilistic Eng. Mech.* **2016**, *43*, 20–35. [[CrossRef](#)]
53. Phan, H.N.; Paolacci, F.; Corritore, D.; Akbas, B.; Uckan, E.; Shen, J.J. Seismic Vulnerability Mitigation of Liquefied Gas Tanks Using Concave Sliding Bearings. *Bull. Earthq. Eng.* **2016**, *14*, 3283–3299. [[CrossRef](#)]
54. D-Amico, M.; Buratti, N. Observational Seismic Fragility Curves for Steel Cylindrical Tanks. *J. Press. Vessel Technol. Trans. ASME* **2019**, *141*, 010904. [[CrossRef](#)]

55. Malhotra, P.K.; Wenk, T.; Wieland, M. Simple Procedure for Seismic Analysis of Liquid-Storage Tanks. *Struct. Eng. Int.* **2000**, *10*, 197–201. [[CrossRef](#)]
56. Baker, J.W. Efficient Analytical Fragility Function Fitting Using Dynamic Structural Analysis. *Earthq. Spectra* **2015**, *31*, 579–599. [[CrossRef](#)]
57. Kitayama, S.; Constantinou, M.C. Probabilistic Seismic Performance Assessment of Seismically Isolated Buildings Designed by the Procedures of ASCE/SEI 7 and Other Enhanced Criteria. *Eng. Struct.* **2019**, *179*, 566–582. [[CrossRef](#)]
58. Malvern, L. *Introduction to the Mechanics of a Continuous Medium*; Prentice-Hall: Englewood Cliffs, NJ, USA, 1969.
59. Hatzigeorgiou, G.D.; Pneumatikos, N.G. Maximum Damping Forces for Structures with Viscous Dampers under Near-Source Earthquakes. *Eng. Struct.* **2014**, *68*, 1–13. [[CrossRef](#)]
60. Tsompanos, A.; School of Pedagogical and Technological Education (ASPETE), Department of Civil Engineering Educators, Athens, Greece. Personal communication, 2 July 2020.
61. Holland, J.H. *Adaptation in Natural and Artificial Systems*; University of Michigan Press: Ann Arbor, MI, USA, 1973.
62. Yang, X.-S. *Computational Optimization, Methods and Algorithms*; Koziel, S., Yang, X.S., Eds.; Springer: Berlin/Heidelberg, Germany, 2011.
63. Calafell, R.L.; Roschke, P.N.; de la Llera, J.C. Optimized Friction Pendulum and Precast-Prestressed Pile to Base-Isolate a Chilean Masonry House. *Bull. Earthq. Eng.* **2010**, *8*, 1019–1036. [[CrossRef](#)]
64. Charmpis, D.C.; Komodromos, P.; Phocas, M.C. Optimized Earthquake Response of Multi-Storey Buildings with Seismic Isolation at Various Elevations. *Earthq. Eng. Struct. Dyn.* **2012**, *41*, 2289–2310. [[CrossRef](#)]
65. Zayas, V.A.; Earthquake Protection Systems, San Francisco, CA, USA. Personal communication, 17 March 2017.
66. Hall, J. The Role of Damping in Seismic Isolation. *Earthq. Eng. Struct. Dyn.* **1999**, *28*, 1717–1720. [[CrossRef](#)]
67. Moeindarbari, H.; Taghikhany, T. Seismic Optimum Design of Triple Friction Pendulum Bearing Subjected to Near-Fault Pulse-like Ground Motions. *Struct. Multidiscip. Optim.* **2014**, *50*, 701–716. [[CrossRef](#)]
68. Barone, S.; Calvi, G.M.; Pavese, A. Experimental Dynamic Response of Spherical Friction-Based Isolation Devices. *J. Earthq. Eng.* **2019**, *23*, 1465–1484. [[CrossRef](#)]
69. Bucher, C. Analysis and design of sliding isolation pendulum systems. *IABSE Symp. Rep.* **2015**, *104*, 1–8.
70. Yenidogan, C.; Erdik, M. A Comparative Evaluation of Design Provisions for Seismically Isolated Buildings. *Soil Dyn. Earthq. Eng.* **2016**, *90*, 265–286. [[CrossRef](#)]
71. Priestley, M.J.N.; Calvi, G.M.; Kowalsky, M.J. *Displacement-Based Seismic Design of Structures*; IUSS Press: Pavia, Italy, 2007.
72. Li, H.; Yu, Y.; Li, J.; Li, Y.; Askari, M. Multi-Objective Optimisation for Improving the Seismic Protection Performance of a Multi-Storey Adaptive Negative Stiffness System Based on Modified NSGA-II with DCD. *J. Build. Eng.* **2021**, *43*, 103145. [[CrossRef](#)]